Published in *Journal of Atmospheric and Solar-Terrestrial Physics* **128**, 105613 (2021)
https://doi.org/10.1016/j.jastp.2021.105613

Quasi-two-day wave characteristics in the mesopause region from airglow data measured at El Leoncito (31.8ºS, 69.3ºW)

Esteban R. Reisin

Instituto de Astronomía y Física del Espacio, Universidad de Buenos Aires - CONICET, Buenos Aires, Argentina

Abstract.

A statistical study of strong quasi-two-day waves (QTDWs) is carried out from the intensities and rotational temperatures of OH(6-2) and O_2b(0-1) emissions measured from the "El Leoncito" Astronomical Complex (31.8ºS, 69.3ºW) between 2006 and 2020. These emissions correspond to layers centered at 87 km and 95 km altitude, respectively. The period, amplitude and phase of each QTDW are obtained after applying rigorous data and spectral conditions. QTDW is the strongest planetary wave in January and is strong during the other summer months. In the rest of the year, the presence of strong QTDWs is more exceptional. Most QTDWs have periods between 45 and 52 hours. In January, the periods are mostly concentrated in the range of 45 to 48 hours, with medians of approximately 46 hours, for both emissions. The peak of QTDW amplitudes is also reached in January, with total averages greater than 10 K for temperatures and 36% (45%) for OH (O_2) relative intensities. Unlike what happens with the semidiurnal tide, there is no increase of the temperature amplitude with altitude: for January there is rather a slight decrease between the OH and the O_2 layer. QTDWs affect airglow intensities more than temperatures, which is reflected in the large Krassovsky's η ratios (with mean vector modulus of 6.14 (±0.15) for OH and 8.08 (±0.11) for O_2). In a high percentage of cases, the vertical wavelength is long (λ_z > 100 km), especially for the O_2 layer. However, waves with λ_z from 20 km were also detected, and with both directions of vertical propagation. The January averages in the documented years (2008-2012, 2014-2015, 2019-2020), indicate the minimum amplitudes (in intensity and temperature) in 2009 and the maximum amplitudes in 2012. For each of the four observed parameters (intensities and temperatures of OH and O_2) there is a different day-by-day evolution of the QTDW amplitudes.

1. Introduction

The quasi-two-day wave (QTDW) with periods close to 48 hours, is one of the main planetary waves present in the mesosphere and lower thermosphere (MLT). Since their early wind observations in the 1970s (e. g. *Clark, 1975*; *Glass et al., 1975*; *Muller and Nelson, 1978*) QTDWs have been extensively discussed in the literature.

Data measured with satellite instruments have been one of the main sources for analyzing the global characteristics of the QTDWs. Measurements made with the "Sounding of the Atmosphere using Broadband Emission Radiometry" (SABER) instrument on board the "Thermosphere – Ionosphere –Mesosphere Energetics and Dynamics" (TIMED) spacecraft have resulted in many publications (e. g., *Palo et al., 2007; Ern et al., 2009; 2013; McCormack et al., 2009; Forbes and Moudden, 2012;*

Pedatella and Forbes, 2012; Gu et al., 2013; 2019; Huang et al., 2013; Chang et al. 2014; Moudden and Forbes, 2014; Nguyen et al., 2016; Wang et al., 2017; Xiong et al., 2018; Liu et al., 2019). Data from the "Microwave Limb Sounder" (MLS) instrument on board the NASA Aura satellite also led to several QTDW papers (*Tunbridge et al., 2011*; *Forbes and Moudden, 2012; Pancheva et al., 2018; Fritts et al. 2019*). Hydroxyl nightglow emission measurements from the "Imaging Absorption SpectroMeter for Atmospheric CHartographY" (SCIAMACHY) onboard Envisat also was used (*Ern et al., 2009*).

QTDWs in the MLT region were also extensively studied with ground-based measurements. Most of the QTDW papers were based on wind data obtained with single radars or radar networks (e. g., *Plumb et al., 1987;Tsuda et al. 1988; Meek et al., 1996; Palo and Avery, 1996; Gurubaran et al., 2001; Jacobi et al., 2001; Namboothiri et al., 2002;* Lima *et al., 2004; Chshyolkova et al., 2005; Nozawa et al., 2005; Pancheva, 2006; Malinga and Ruohoniemi, 2007; Tunbridge and Mitchell, 2009; Hecht et al., 2010; Suresh Babu et al., 2011; Guharay et al., 2012; 2015; Lilienthal and Jacobi; 2015; Ma et al., 2017; Venkateswara Rao et al., 2017; Xiong et al., 2018; Fritts et al., 2019; Gaikwad et al., 2019*).

In contrast to radar data, QTDW studies using data obtained with other types of ground-based instruments are very scarce. There are a few studies which use airglow data (*Takahashi et al., 2005; López-González et al., 2009; Hecht et al., 2010)* . Here some features of the QTDW will be obtained, using a large airglow data set observed at El Leoncito, in the Argentine Andes. The description of the data and the spectral analysis method used to detect and quantify the QTDWs are described in Section 2. The QTDW results are presented in Section 3, while these are compared with the literature in Section 4. The main results are highlighted in Section 5.

2. Data and analysis method.

The Argentine Airglow Spectrometer (AAS) measures, in the zenith direction, band intensities and rotational temperatures of OH (6-2) and O_2b (0-1) emissions (*Scheer, 1987*; *Scheer and Reisin, 2001*), whose layers are centered nominally at 87 km and 95 km altitude, respectively (e. g., rockets observations by *Baker and Stair Jr., 1988*; *Witt et al., 1979*). The set of these four parameters (and the spectral background) is measured approximately every 80 s. In April 1998, the instrument was automated and continues measuring from the Astronomical Complex "*El Leoncito*" (CASLEO, 31.8ºS 69.3ºW) with some interruptions due to instrumental failures (see table of number of nights with data per month and year http://www.iafe.uba.ar/aeronomia/Months.html).

In principle, the data from January 2, 1998 to February 4, 2020 are used for the present analysis. However, due to the strict selection criteria applied for this analysis (see below), the first results correspond to February 2006 (with two exceptions in December 2002), when the sequence of many consecutive nights with data began to be frequent.

In order to reduce the spectral noise due to fast oscillations, for each of the four parameters measured, the averages of the 30-minute bins are used (a minimum of 10 data is required for each bin). Spectral analysis is performed on windows of 17 consecutive nights. As a quality requirement, only windows that have data every night and with an average of at least 4 hours of data per night are used. After testing with different window lengths (6, 11, 15, 16, 17, 18 and 20 days), the 17-day length was chosen because it had the highest rate of QTDWs detected per window.

Despite the strict selection criteria mentioned above, more than 2600 windows for each parameter were analyzed. Here, each window is labeled with the date of the central night (e. g., the January 8, 2015 window, is the one that includes the nights from January 1 to 17, 2015). The number of windows is well distributed in every month, with between 132 and 255 windows depending on the month (see Fig. 1).

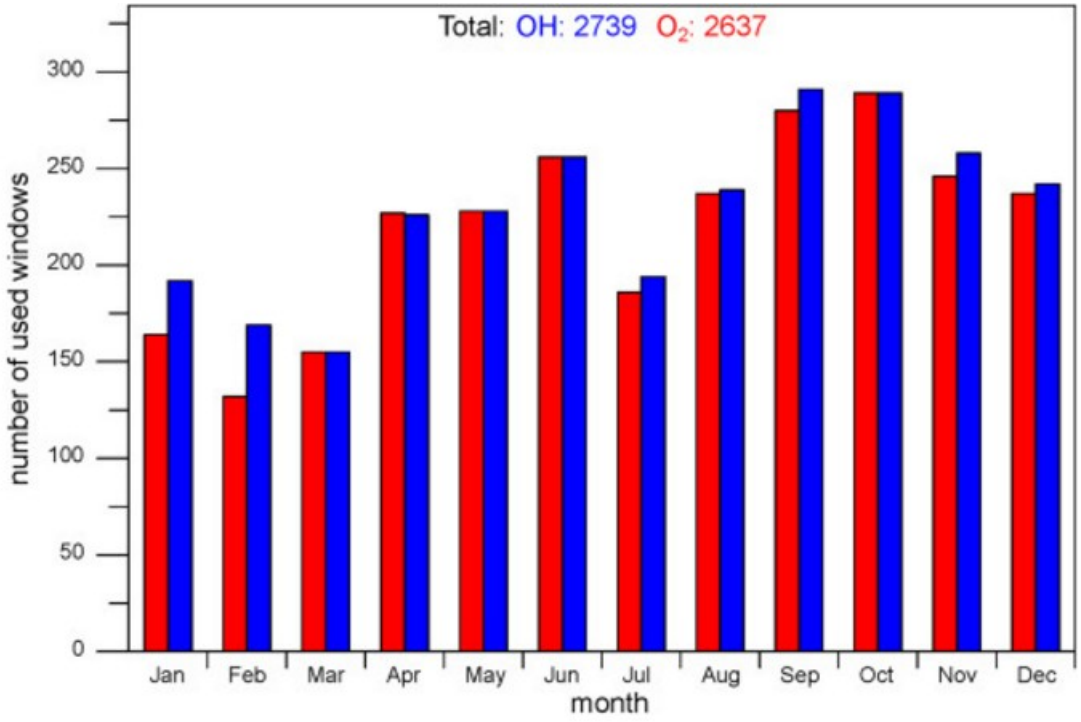

Fig. 1. Number of 17-day windows per month used in the present analysis for OH (blue) and O_2 (red).

These windows, of course, are not independent, as neighboring windows share 16 data nights. Despite this data overlay, the results of each data window are obtained separately. In this way, a better statistical quality is obtained for the mean values (e. g., monthly average amplitudes) than if only windows without overlapping nights were used. An additional advantage of this overlay approach is that it allows the day-to-day evolution of the QTDW to be followed. Case count histograms are also shown below. Since most cases are not independent, the case count is not the same as the QTDW event count. The number of cases in the histograms can be considered as a measure of the presence level of strong QTDWs. These histograms are then used as a proxy for the discussion of some aspects of the QTDW.

The 17-day length of the windows is suitable to study planetary waves of different periods. Here the analysis is limited to windows where QTDW is strong. For this, the period, amplitude and phase are calculated with the sinusoidal fit by least squares already used in the past (e. g. *Reisin and Scheer*, 1996; 2019) thus obtaining the main spectral component. The second spectral component is also obtained, applying the sinusoidal fit to the remainder of the data after subtracting the sinusoid from the main spectral component. To study QTDW, only cases in which the period is within the range of 1.6 to 2.4 days (38.4 to 57.6 hours) are considered. In addition, it is required that the calculated periods of intensities and temperatures be similar, with a difference of no more than one hour. An example of a QTDW in the four observed parameters is shown in Fig. 2. The 30-minute data averages between January 6 and 22, 2011 are contrasted with the reconstruction curves of the two main sinusoids. It is seen how the

slow variations of the data are well represented by their respective fits (note that the "noisier" shape in the TO2 curve is due to the fact that the second spectral component has a short period (0.34 d) that is not present in the other three parameters).

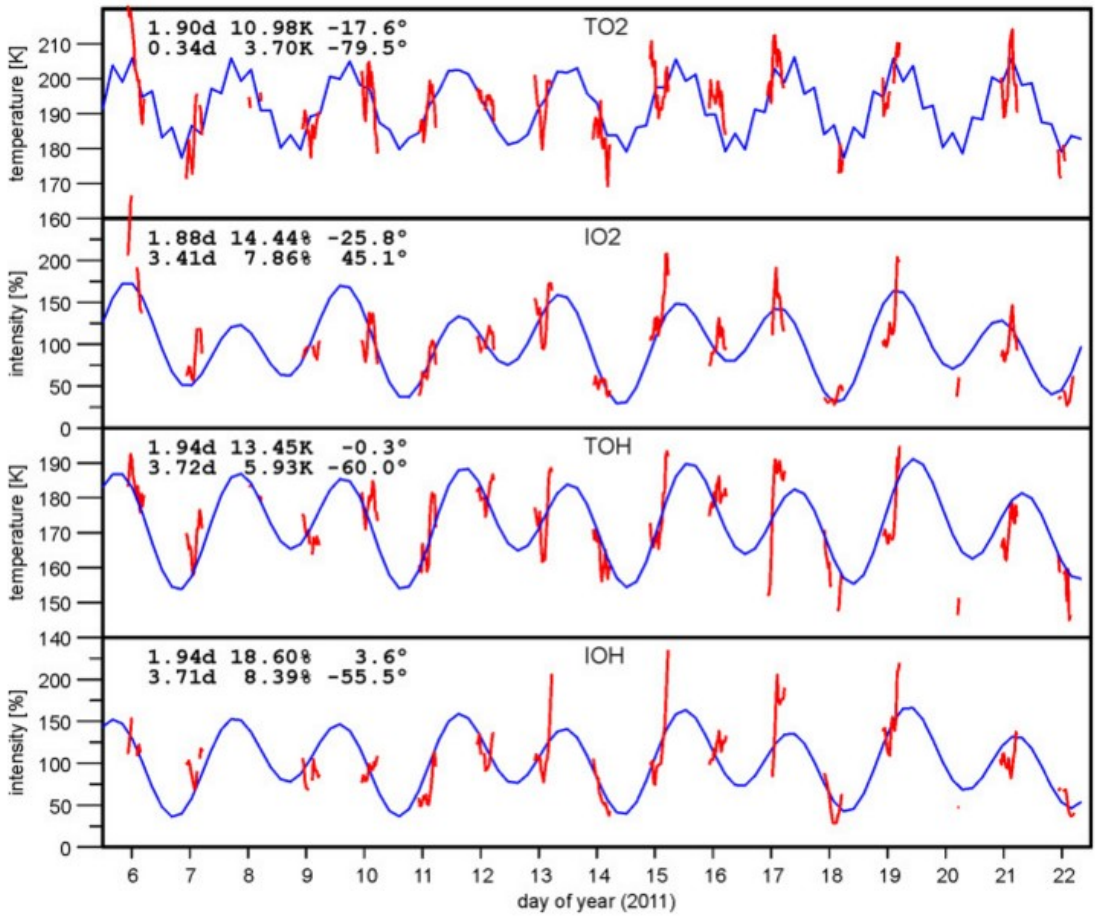

Fig. 2. 30-minute data averages, measured by the AAS between January 6 and January 22, 2011. From top to bottom: O_2 temperatures, O_2 intensities, OH temperatures, and OH intensities. The least squares fits of the two main spectral components are also shown. The periods, amplitudes, and phases of these components are also indicated on the left top of each frame.

The characteristics of the vertical wave propagation are obtained using the theory of *Hines and Tarasick* (*1987*). According to this theory, for airglow zenith measurements, the vertical wavelength and the direction of propagation depend on the Krassovsky's η ratio. This ratio is a complex dimensionless number defined as

$$\eta = \frac{A_I / I}{A_T / T} e^{i\phi},$$

where A_I and I are the nocturnal amplitude and mean intensity, A_T and T the corresponding values for temperature, and ϕ is the difference of the intensity and temperature phases ($\phi = \phi_I - \phi_T$). The phase ϕ is evaluated at the center of the data window to avoid systematic errors due to the small differences of the intensity and temperature frequencies. The vertical wavelength is (see *Reisin and Scheer*, *1996*)

$$\lambda_z \approx \frac{2\pi\gamma H}{(\gamma - 1)\eta \sin\phi},$$

where γ = 1.4 is the ratio of the specific heats and H the scale height. A sign to λ_z is attached, so that a negative λ_z means downward propagation of wave phase (or upward energy propagation), and of course the opposite for positive λ_z. For long vertical wavelengths, the phase varies little with altitude and, due to the margin of error, it is difficult to distinguish whether the wave is ascending, descending or even evanescent. As was done in previous papers (e. g., *Reisin and Scheer, 1996; 2019*), here the condition $|\lambda_z| > 100$ km is used to refer to "long vertical wavelength" waves, for which the direction of vertical propagation is not clearly defined.

3. Results.

From the present data analysis, it turns out that the QTDWs are evidenced in 221 cases for the O_2 emission, and in 169 cases for the OH emission. This is 8.4% and 6.1% of the total 17-day windows analyzed, respectively. Of special interest are the 78 cases in which QTDW are well documented in the two emission layers simultaneously.

The monthly distribution of cases shows a clear peak in January, which is greatly reduced in the neighboring months of December and February (see Fig. 3a). The remaining months have few cases and almost none that are simultaneous in both emissions. The preponderance of cases in January is more evident if only the main spectral components are considered (see Fig. 3b). Note that, in addition, January is one of the months with the fewest analyzed windows (Fig. 1). For this month, the QTDWs were detected in 47% and 58% of the windows for OH and O_2, respectively. These percentages remain high, even if the cases are limited only to the main spectral component (38% for OH, 50% for O_2). Note that the periods of sinusoidal fits are *not* restricted to the range close to 2 days (see example in Fig. 2). Since only the main spectral components are used, this means that the detected cases of QTDW have amplitudes that exceed any other planetary wave that might be present. From the fact that for January, the QTDW is detected in at least half of the windows in O_2 (and a somewhat lower percentage in OH) it can be concluded that the QTDW is the strongest planetary wave during this month.

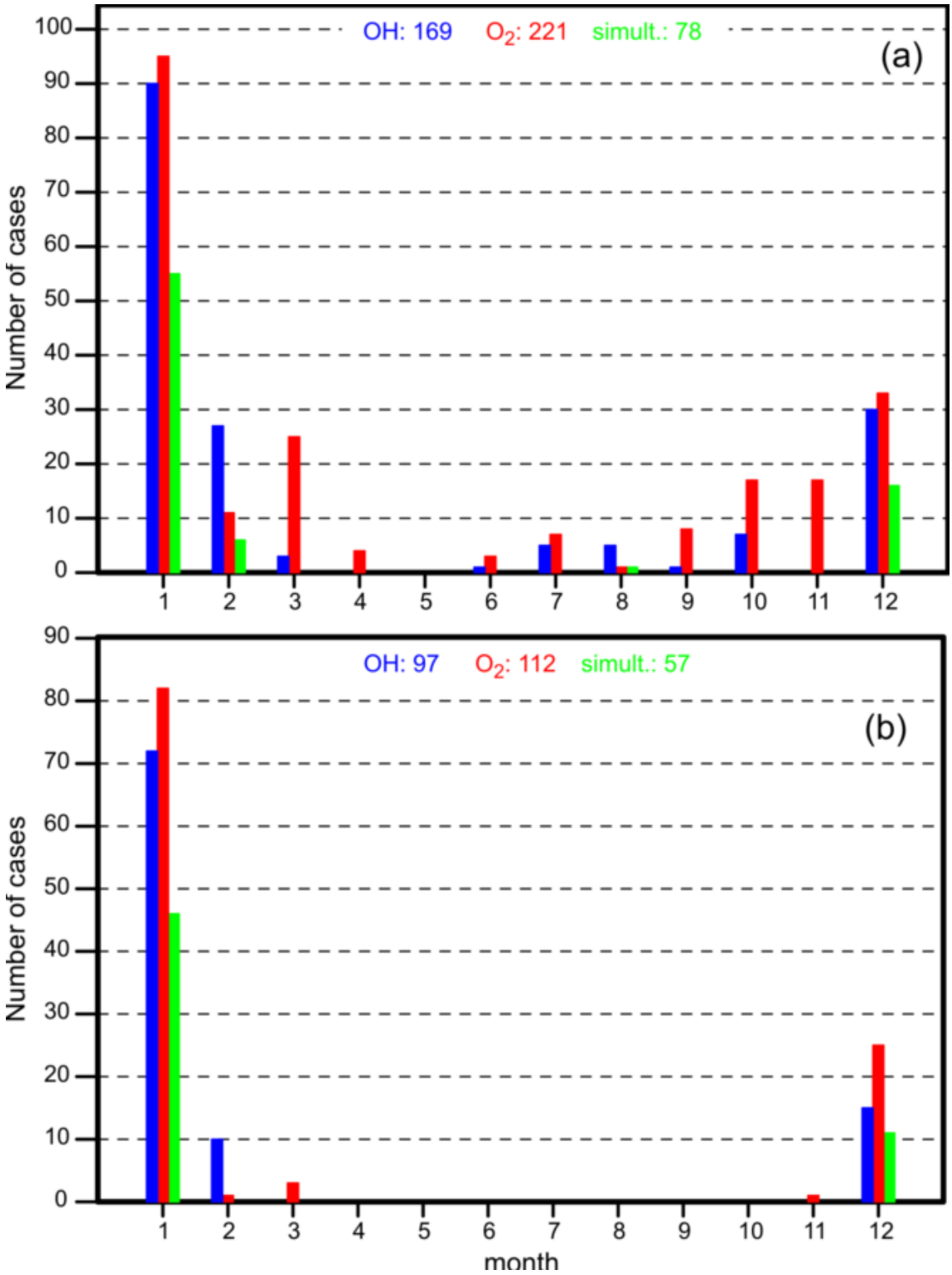

Fig. 3. Monthly distribution of detected QTDW cases, for OH emission (blue), O_2 emission (red) and simultaneous in both emissions (green): using two spectral components per window (a); and using only the main component (b).

In the two emissions, the periods tend to be slightly less than 2 days. Most cases occur between 45 and 52 hours (see Fig. 4a), with 68% of OH cases and 70% of O_2 and medians of 47.1 and 46.2 h, respectively. Limiting itself to 78 simultaneous cases, the concentration of cases in this period range is even higher, with 81% of OH cases and 77% of O_2 cases (and the corresponding medians of 46.1 h and 45.7 h).

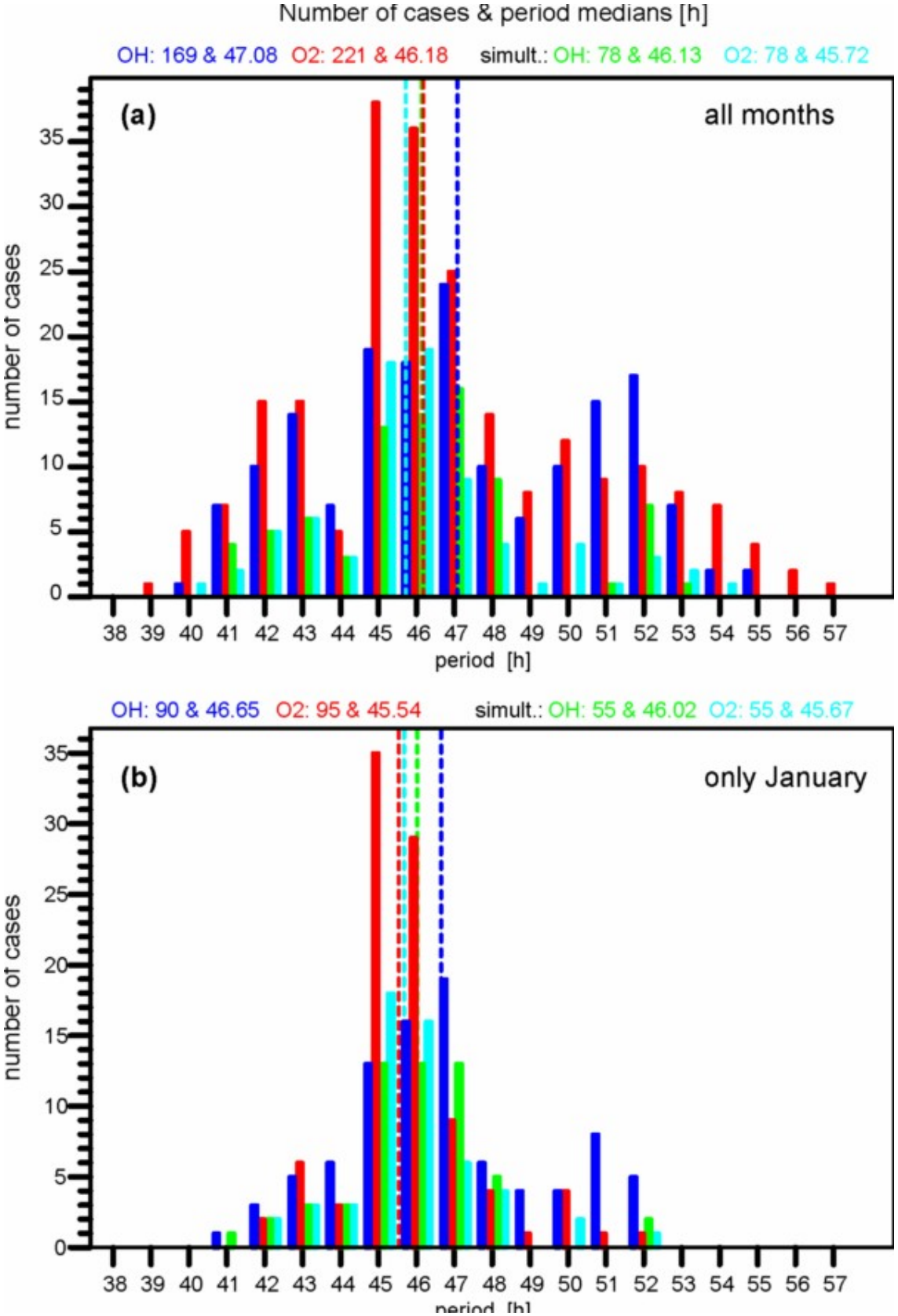

Fig. 4. Histogram of the QTDW periods for OH (blue), O_2 (red), simultaneous for OH (green), and simultaneous for O_2 (cyan): All cases (a) and only January cases (b). Medians are indicated by the vertical dashed lines.

January is the month with the highest temperature amplitude averages, exceeding 10.4 K in both emissions (Fig. 5). The neighboring months December and February have

smaller averages, around 7 K. The other months, much less documented, have monthly averages below 6 K.

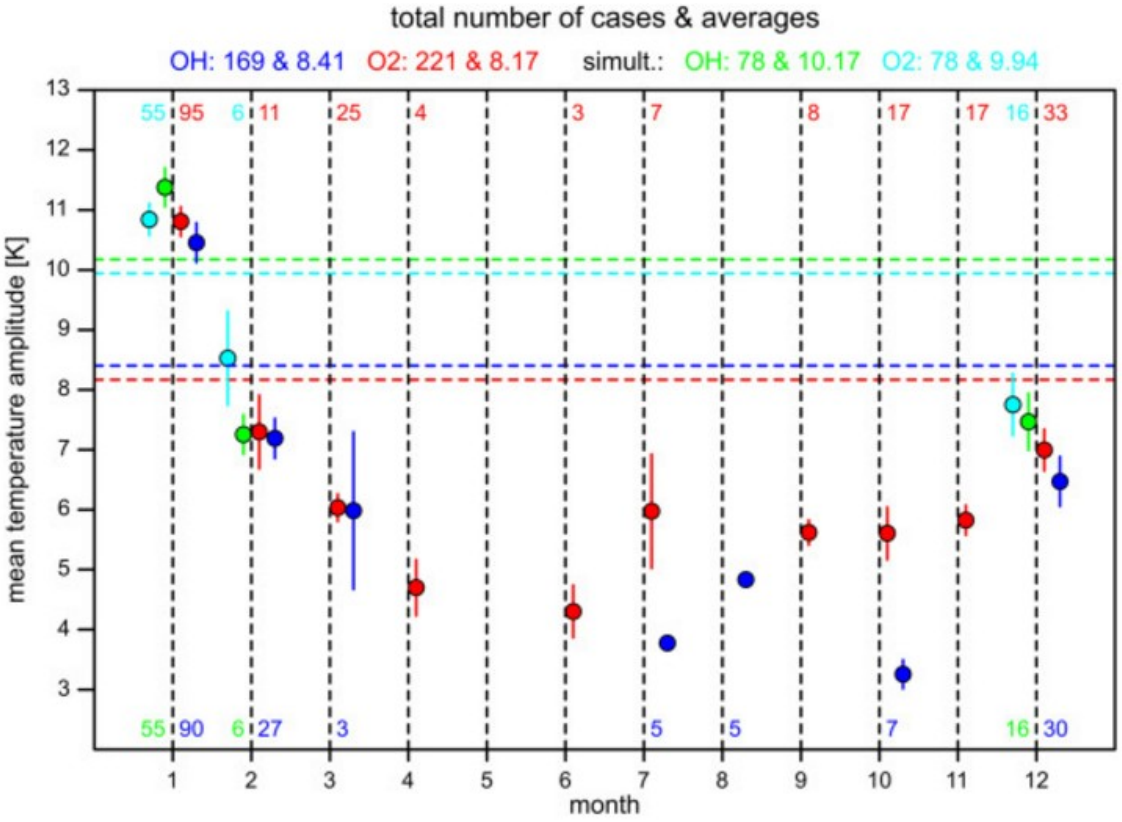

Fig. 5. Monthly averages of temperature amplitudes. Same color code as in Fig. 4. The numbers near the vertical dashed lines indicate the number of cases used for each monthly average. Total averages are indicated by the horizontal dashed lines.

Monthly averages of the amplitude of relative intensity (with respect to the window mean) also peak in January (36% for OH and 43% for O_2, see Fig. 6). The neighboring months of December and February have somewhat lower monthly averages, from 22% to 34%.

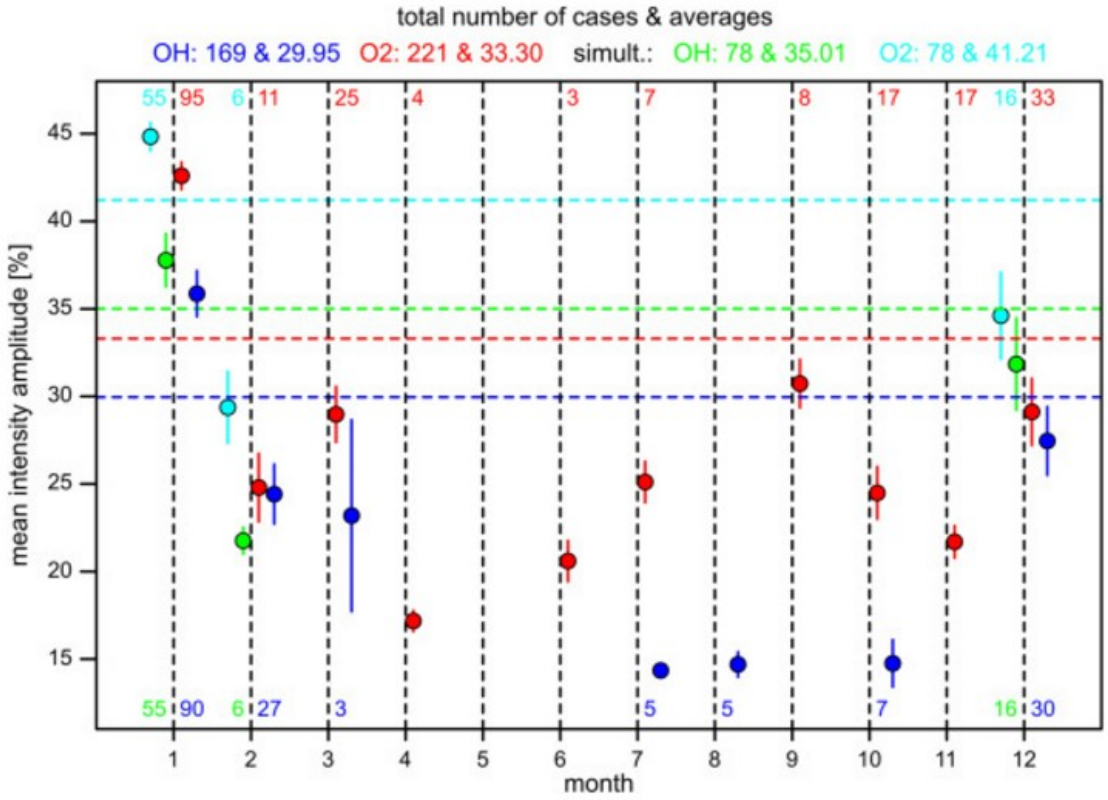

Fig. 6. Same as Fig. 5, but for relative intensity amplitudes.

All Krassovsky's η values are located in the first and fourth quadrants of the complex plane (see Fig. 7). Many of the points are close to the real axis, *i.e.*, intensity and temperature oscillations are almost in phase. This η behavior is very different from the case of the semidiurnal tide, where the η points are clearly located only in the fourth quadrant (*Reisin and Scheer, 2019*). The modulus of η tend to be larger for O_2 than for OH. The mean vector for O_2 is $|\eta| = 8.08(\pm 0.11)$, $\phi = -3.80^{o}(\pm 0.79^{o})$; and for OH is $|\eta| = 6.14(\pm 0.15)$, $\phi = 0.02^{o}(\pm 1.44^{o})$.

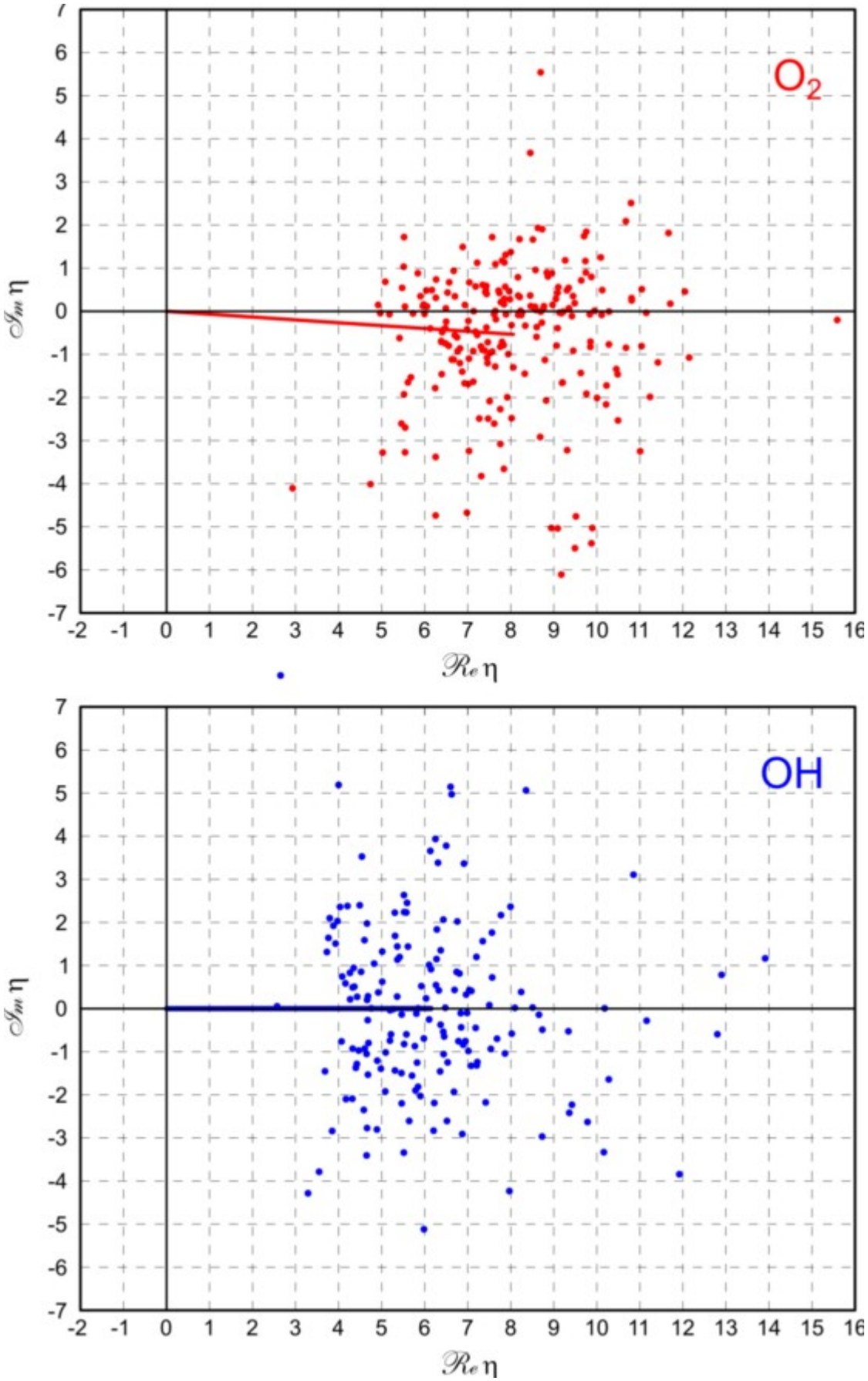

Fig. 7. Krassovsky's η ratio of the QTDW in the complex plane, for O_2 (top) and OH (bottom). The respective average vectors are also shown.

For O_2 emission, most QTDWs have a long vertical wavelength, so they do not have a clear vertical propagation direction defined. There are 70% of cases with $|\lambda_z| > 100$ km. (Fig. 8). For OH emission, the number of cases with a long vertical wavelength is less (47%). For the simultaneous cases, these percentages are 72% for O_2 and 38% for OH, that is, the vertical wavelength tends to be shorter in the lower altitude emission layer.

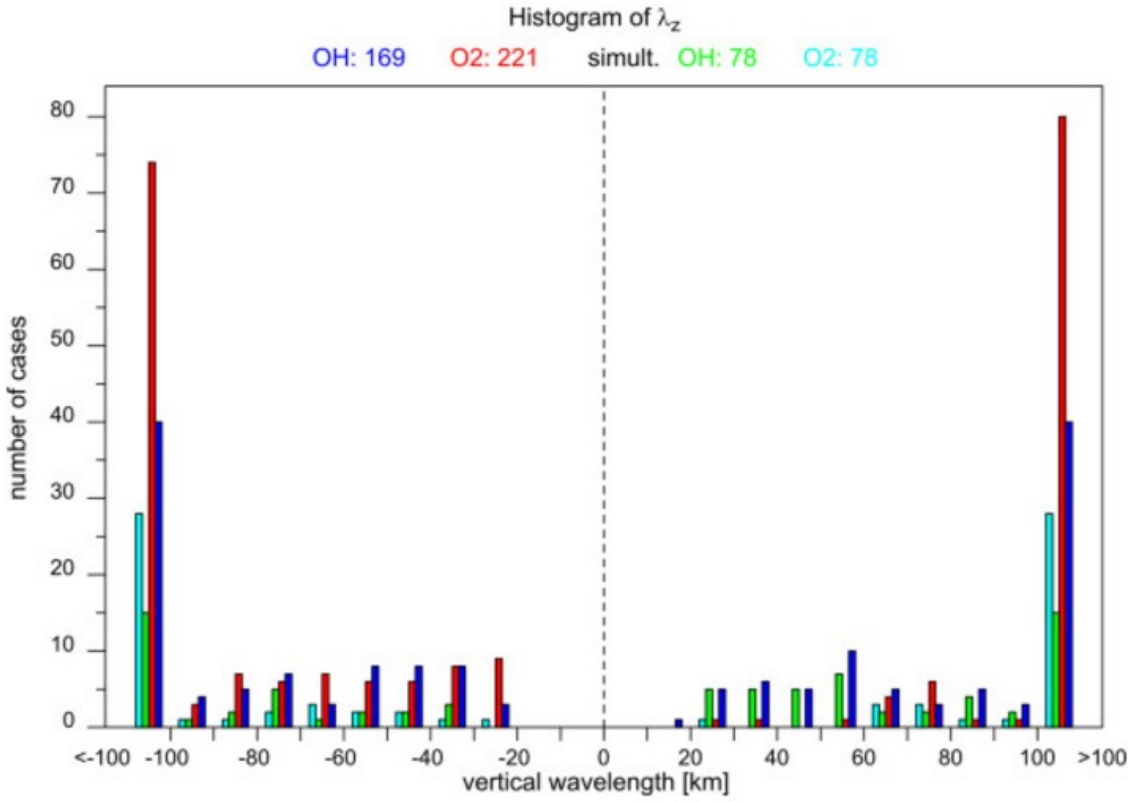

Fig. 8. Vertical wavelength distribution of the detected QTDWs. Same color code as in Fig. 4. The cases with a long vertical wavelength are accumulated in the leftmost (λ_z < -100 km)) and rightmost (λ_z > 100 km) bars group.

From what has been discussed so far, one can see that during January, QTDW is often the strongest planetary wave. During the other months of the year, the occurrence of strong QTDWs is much less frequent. In what follows, only the January cases will be considered to analyze the interannual variation of the QTDW. The distribution of QTDW periods for January (Fig. 4b) is clearly more concentrated than the distribution for all months (Fig. 4a). Nearly all January cases are included between 42 and 52 hours. Only in the reduced 45 h - 48 h range occur 60% of OH cases and 81% of O_2 cases, while for simultaneous cases these percentages are 80% in both emissions.

There are nine years with monthly averages for January available (from 2008 to 2020), six of which are for both emission layers (starting from 2011). The temperature amplitude averages of OH range from 5.0 K to 12.6 K, indicating a strong variation from year to year (Fig. 9). The amplitude of the O_2 temperature variations is reduced to the range from 9.1 K to 14.1 K. For both emissions, the year with the highest temperature range was 2012, with mean values greater than 12 K. The lowest values correspond to 2009 and 2010, but only the OH amplitudes are documented. For each year, the temperature amplitude average of the simultaneous cases do not differ significantly from the amplitude average of all the cases: The only exceptions are for OH temperatures in 2020 and 2014 with differences of 1.9 (±0.9) K and 1.6 (±1.1) K,

respectively. Furthermore, from the simultaneous cases, it follows that the temperature amplitudes in the two emission layers are similar, only slightly higher for OH. This is most evident with the ratio of temperature amplitudes of O_2 over OH (Fig. 10) with a six-year average value of 0.95 (±0.04).

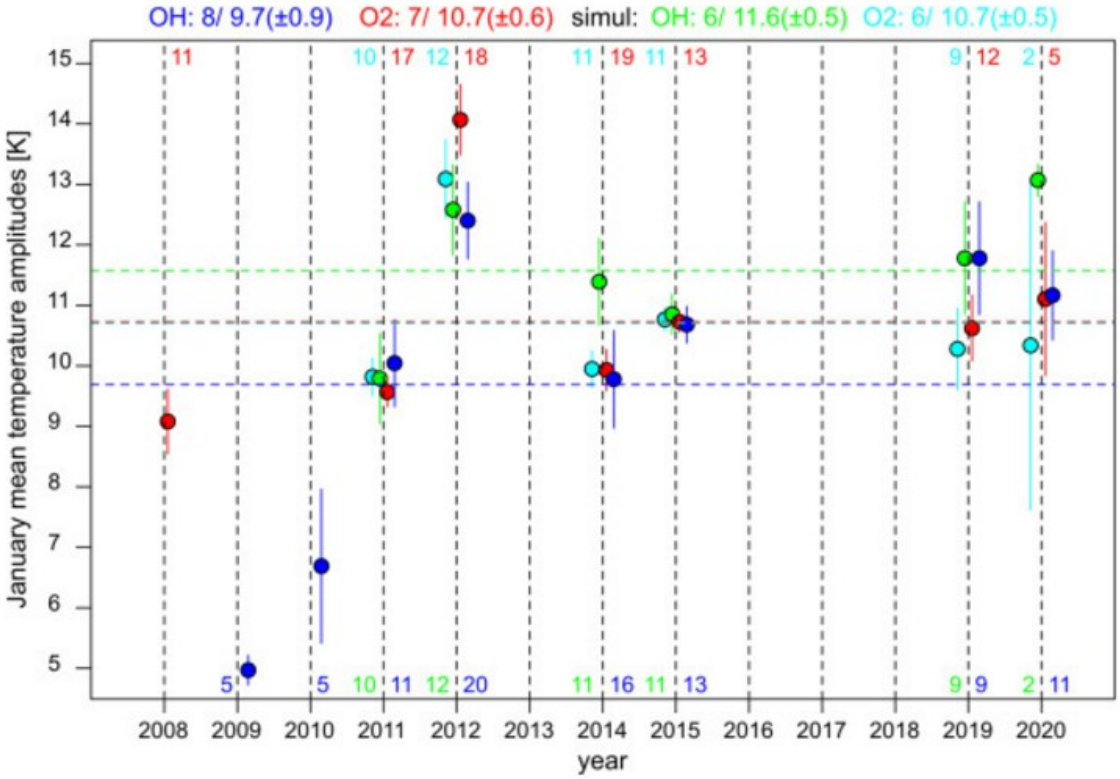

Fig. 9. January average temperature amplitudes for each year. Same color code as in Fig. 4. The number of 17-day windows used in each average is also indicated near the corresponding vertical dashed lines. The total averages are shown with the horizontal dashed lines and numerically at the top. Note that the scale starts in 2008, because there was not enough data in the January prior to this year.

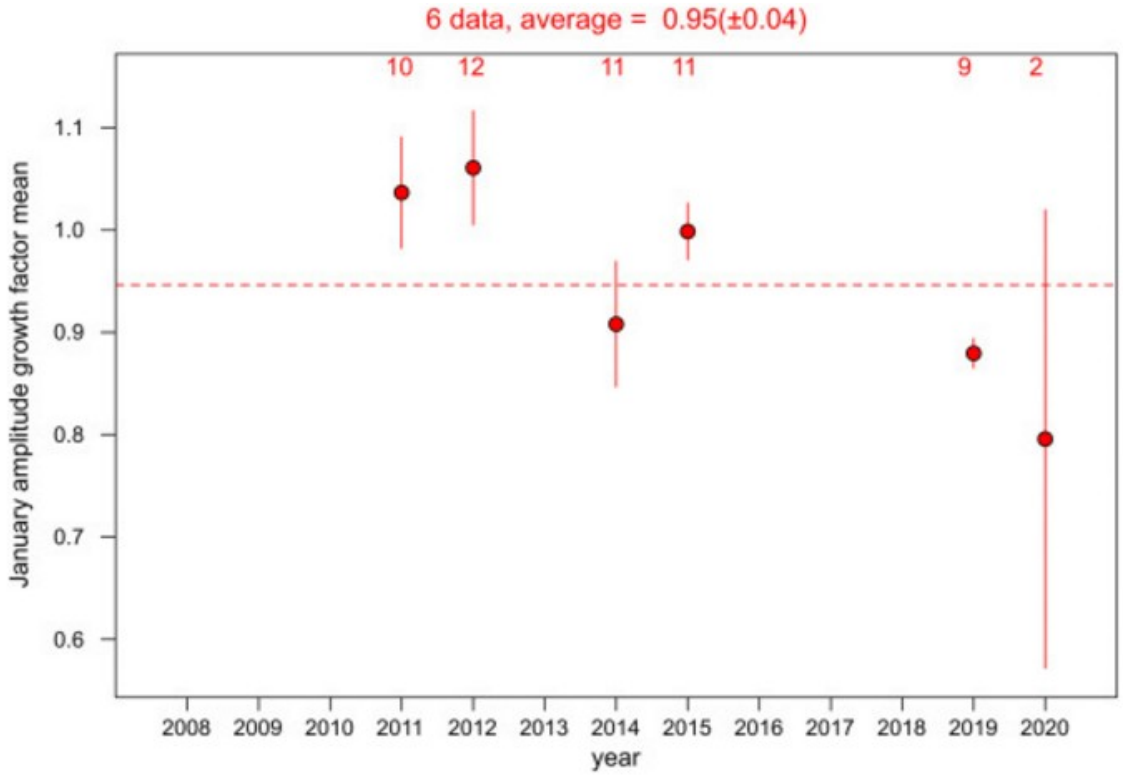

Fig. 10. January averages of the temperature amplitude growth factor (A_{TO2} / A_{TOH}). The average of the 6 documented years is indicated with the horizontal dashed line.

In January, the amplitude of the relative intensity is usually very strong and variable from year to year. January averages range from 27% to 49% (with the exception of 2009 for OH (18%); see Fig. 11). On average, the relative amplitudes of O_2 are about 23% greater than those of OH. From Figs. 9 and 11, it can be seen that the year-to-year amplitude variations for temperatures and intensities are somewhat different. However, they have in common the minimum of OH in 2009 and the maxima of OH and O_2 in 2012.

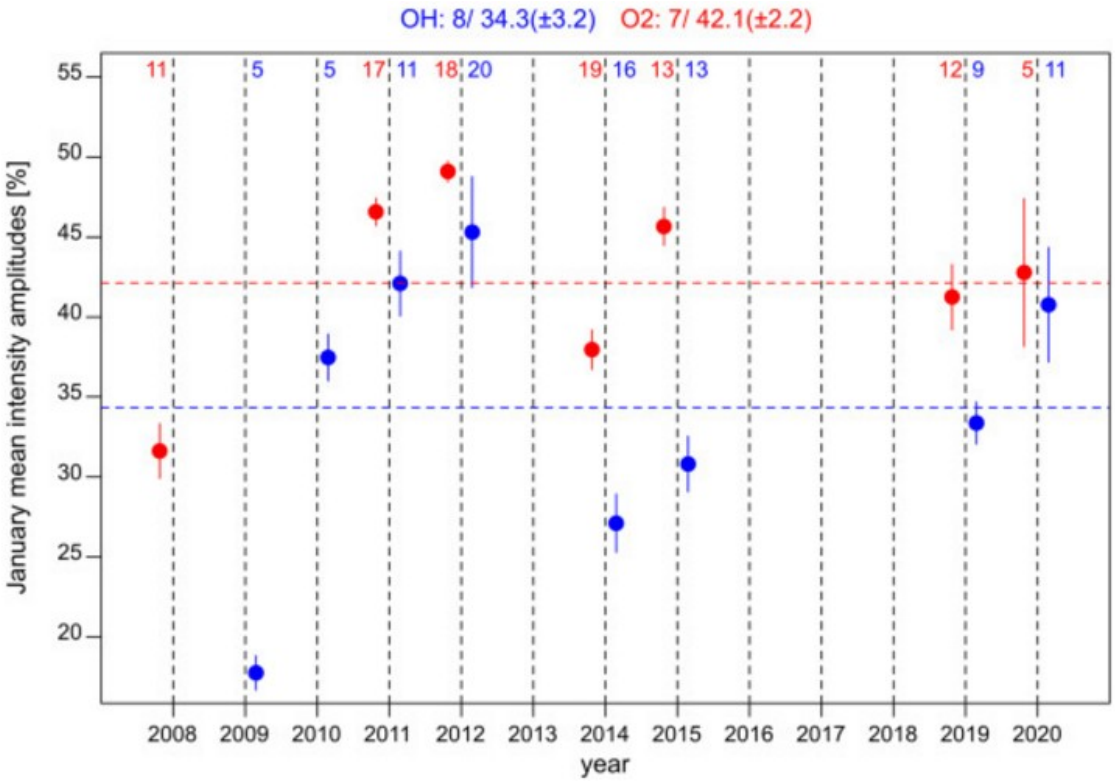

Fig. 11. Same of Fig. 9, but for relative intensity amplitudes.

It is interesting to see how the QTDW temperature amplitudes evolve within January 2012, which is the best documented year. For OH, the maximum amplitude is reached on January 6, lasting until at least January 8 (between 10 and 14 there are no data). Already on January 15 the amplitude is much less and tends to drop until 31 inclusive (Fig. 12). For O_2, the amplitude peak is delayed between 4 and 6 days with respect to OH: The maximum is on January 12 (although it could have been reached up to two days before) and lasts until January 15. From January 16, the amplitudes decrease almost continuously to less until January 23. As in previous papers (e. g. *Reisin and Scheer, 2019*), the error bars in Fig. 12 (and also in Figs. 13, 15 and 17) were calculated with the jackknife method (*Efron and Gong, 1983*).

In January 2012, the amplitudes of O_2 relative intensity remained fairly constant between day 1 and 22 (Fig. 13). In a different way, for OH, the amplitude tends to attenuate throughout the month. Furthermore, these day-to-day evolutions in the intensities are very different from the evolutions in the temperatures (see Fig. 12). Although only the amplitudes of January 2012 are shown here as an example, significant differences in the temporal evolution between the four measured parameters were observed in the other years.

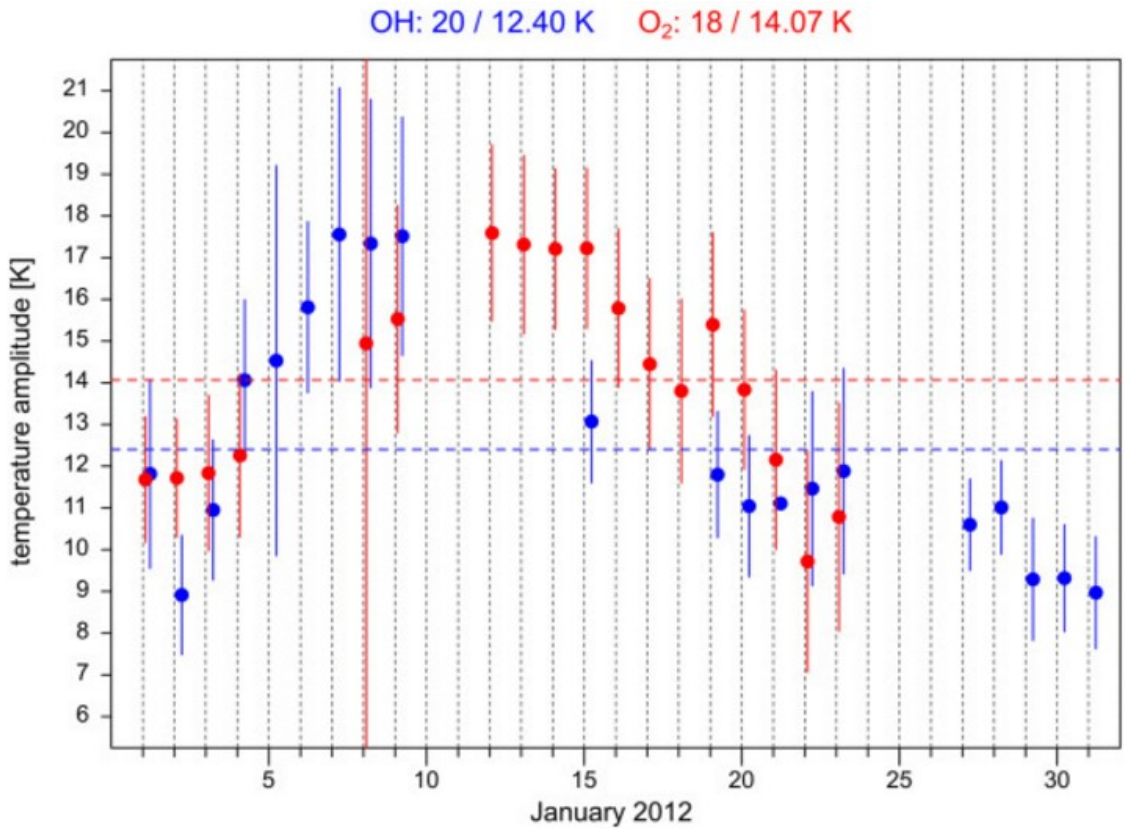

Fig. 12. Day-to-day evolution of the QTDW temperature amplitude during January 2012, for OH (blue) and O_2 (red).

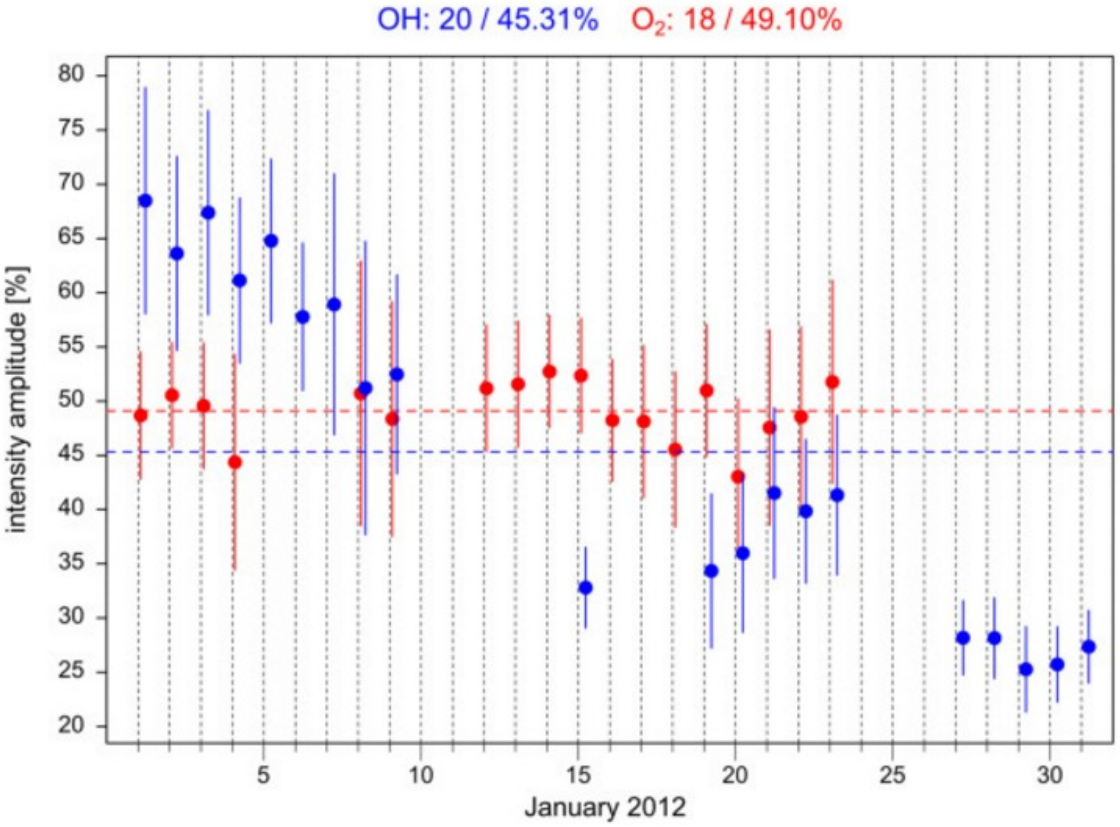

Fig. 13. Same of Fig. 12, but for relative intensity amplitudes.

As already mentioned, the vertical wavelength tends to be long, especially in the O_2 layer. This can also be seen in the January vertical wavenumber averages ($k_z = 1/\lambda_z$; see Fig. 14). In the O_2 layer, all January averages (expressed in wavelength) have a modulus greater than 100 km. This is also the case for most years in the OH layer, the exceptions are in 2011 and 2015 with λ_z averages of 34 km and 70 km, respectively (the 2019 average includes λ_z > 100 km within the margin of error).

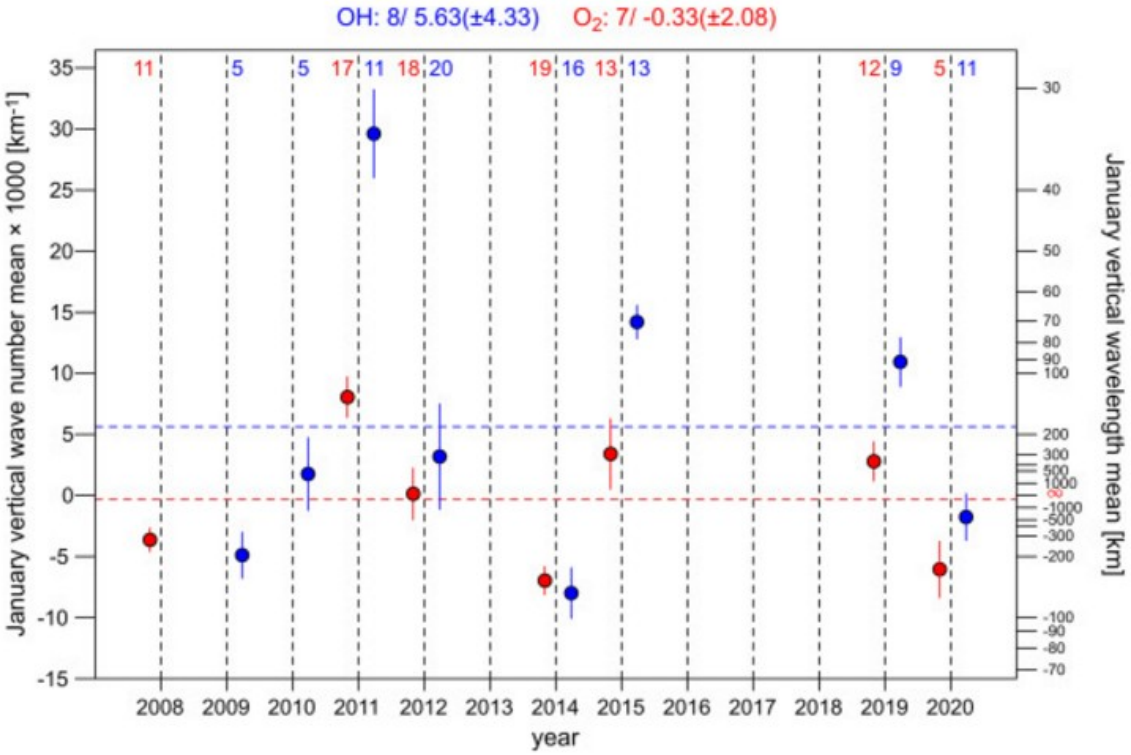

Fig. 14. January averages of the vertical wavenumber ($k_z = 1 / \lambda_z$) versus year, for OH (blue) and O_2 (red). Total averages are indicated by the horizontal dashed lines. The vertical wavelength scale is displayed on the right hand side.

The temporal evolution of λ_z during January 2012 is different depending on the emission layer. In the O_2 layer, the vertical wavelength is long on almost all available days of the month, except for January 9 and 12 (Fig. 15). In contrast, the vertical wavelength is much more variable in the OH layer: On January 1-3, the energy propagation is upward, on January 4-15 and 27-31, $|\lambda_z|$ it is long, and on January 19-23 the energy propagation is downward.

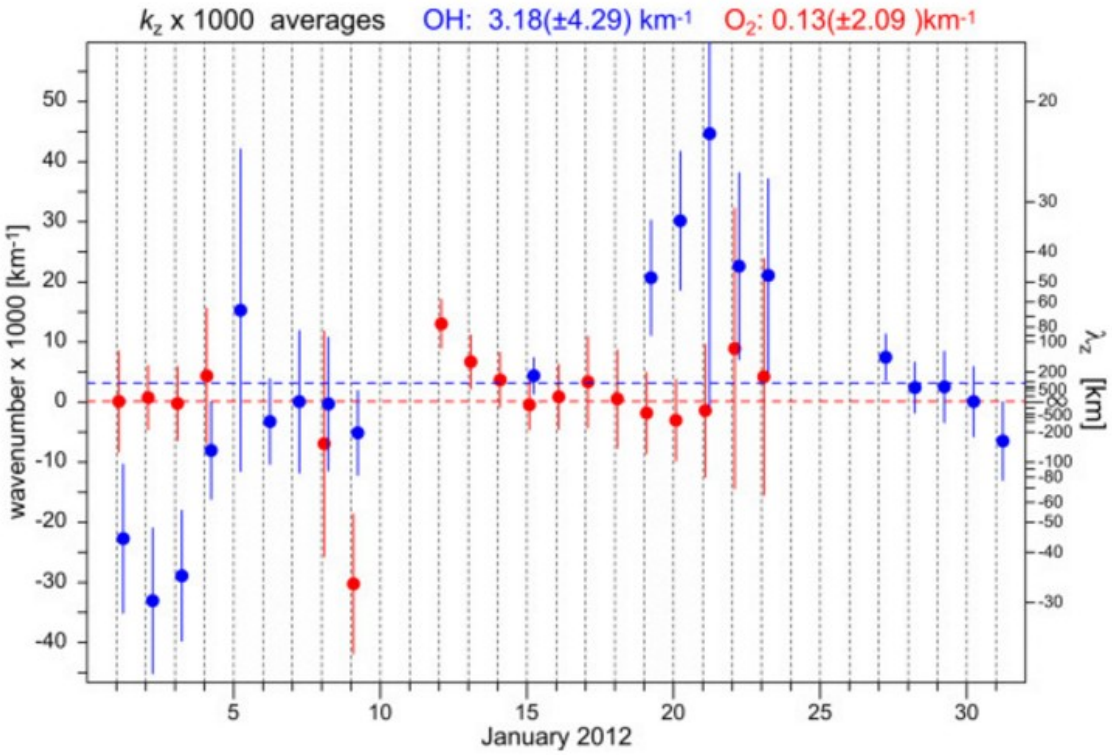

Fig. 15. Day-to-day evolution of the QTDW vertical wavenumber during January 2012, for OH (blue) and O_2 (red).

The long vertical wavelengths can also be seen in the phase comparison between the two emission layers. Fig. 16 shows the January averages of the O_2 minus OH phase differences $\Delta\phi$, for temperatures and intensities. The averages are consistent with zero offset, or somewhat positive (that is, the oscillation in the upper layer is ahead of the oscillation in the lower layer). For the 55 windows involved, the total average of $\Delta\phi$ is only +3.42 (±0.28) h for temperatures and +1.85 (±0.42) h for intensities, which represents about 14% and 8% of the maximum possible phase difference for 48-hour period wave, respectively. The maximum phase difference of 5.4 h is reached for temperatures in 2012. The temporal evolution of the phase differences during that January is different for temperatures and intensities: while for temperatures, the $\Delta\phi$ values vary without a clear trend between 3 and 6 hours, for intensities, they tend to decrease during the month from 8 to 0 hours (Fig. 17).

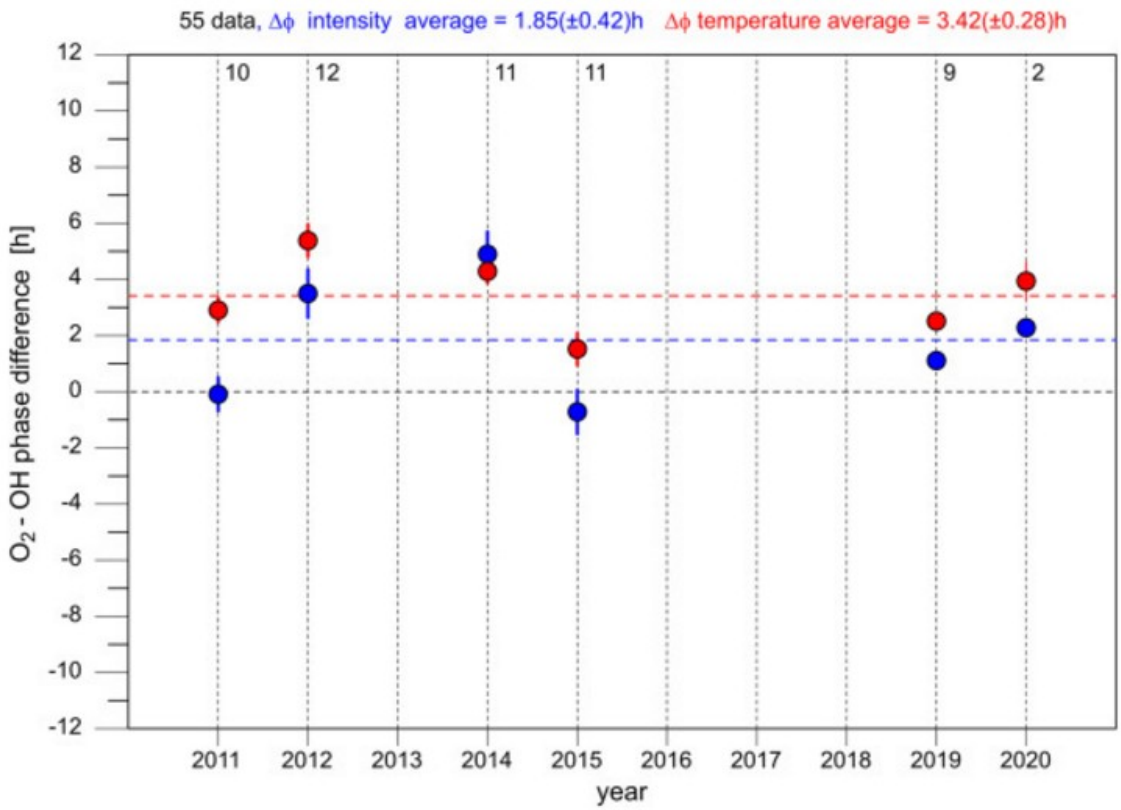

Fig. 16. January averages of the phase differences of the QTDW ($\Delta\phi = \phi_{O2} - \phi_{OH}$), for relative intensities (blue) and temperatures (red). Total averages are indicated by the horizontal dashed lines.

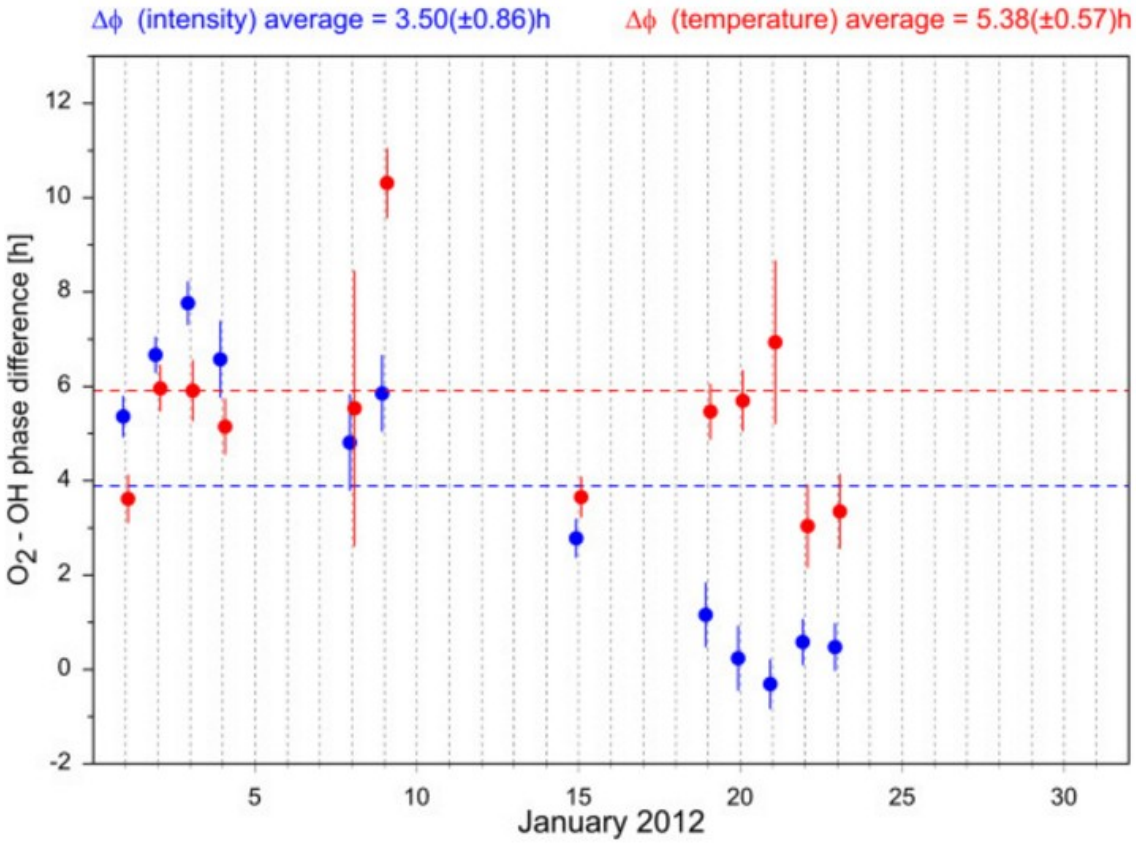

Fig. 17. Day-to-day evolution of the phase differences $\Delta\phi$ during January 2012. Same color code as Fig. 16.

4. Discussion

Our results based on airglow data show an evident preponderance of quasi-two-day waves during the summer months, especially in January. During the rest of the year, the presence of QTDWs is much weaker, and does not stand out over the other planetary waves. This seasonal behavior is widely recognized in the literature for midlatitudes of the Southern Hemisphere (SH; e. g. , *Hecht et al., 2010;,Yue et al., 2012; Gu et al., 2013; 2019; Huang et al., 2013; Pancheva et al., 2018*).

From our measurements located at a single site, it is not possible to discern which zonal modes are involved in the observed QTDWs. Models, satellite observations, and ground-based instrument networks agree that the westward propagating zonal wavenumber 3 (W3) is usually the dominant QTDW mode in summer SH midlatitudes (*Salby, 1981*, *Ern et al., 2009; Tunbridge et al., 2011 ; Pendlebury, 2012; Pedatella and Forbes, 2012; Pancheva et al., 2018; Fritts et al., 2019; Gu et al., 2019; Liu et al., 2019*). Other QTDW modes, such as westward wavenumber 2 and 4 (W2 and W4) or eastward wavenumber 2 (E2) are also discussed in the literature, although in general, their amplitudes are lower than those reached by W3 mode.

As mentioned, most of the QTDWs observed here are limited to a period range of ±4 h around 48 h. For January only, the periods are even more concentrated in both emission layers, with medians around 46 h. The tendency to periods somewhat shorter than 48 h may be related to the phase-locked 2-day waves, discussed by *Walterscheid and Vincent (1996).* Moreover, these periods tend to be shorter than the value of 2.1 days mentioned by *Salby* (*1981*). Using MLS data from January 2015, *Fritts et al. (2019)* determines a range of periods between 44 and 52 h, similar to what is observed here. In the same

sense, with SABER temperatures, *Moudden and Forbes (2014)* find periods ranging between 43 and 52 h for the SH. Also with SABER data for the austral summer, *Gu et al.* (*2019*) found that the W2 mode of QTDWs are more frequently observed with periods between 45 and 48 h, the W3 mode between 45 and 52 h and the mode W4, between 41 and 56 h. *Guharay et al. (2015)* , with wind data obtained with a meteor radar in Cachoeira Paulista (22.7ºS 45ºW) between 2000 and 2014, observe much wider QTDW period range, between 36 and 70 h. The 20-year simulation based on Canadian Medium Atmosphere Model (CMAM) by *Pendlebury (2012)*, predicts QTDW periods from 1.5 days. This contrasts with the present results, since almost no cases with periods shorter than 40 h have been observed.

El Leoncito is located within the zone between 30ºS and 40ºS, where the W3 mode of the QTDW reaches a maximum amplitude (*Liu et al., 2019*). The temperature amplitudes of the QTDWs are strong in January, with total averages above 10 K, while in December and February the amplitudes are approximately 3 K lower. For January 17, 2015, *Fritts et al. (2019)* show that the temperature amplitude of the strongest westward wave mode 3 is around 8 K, at 30ºS and 80-100 km altitude (see their Fig. 12). This value is somewhat less than the January 2015 average amplitudes of ~10.7 K determined here for both emissions (Fig. 9). For the same W3 wave mode, month, latitude and altitude range, *Gu et al. (2019)* derives amplitudes between 8 and 14 K (see their Fig. 1d) that are values similar to those obtained here.

Gu et al. (2013) show the QTDW January temperature amplitudes obtained with SABER between 30ºS and 40ºS from 2003 to 2012 (see their Fig. 6). The years with the weakest amplitudes (for W3 wave mode) were 2008, 2009 and 2010, never exceeding 8 K in the mesopause region. In the other years the amplitudes are much higher, especially in 2011 and 2012, when the amplitudes reached 14 K. *Moudden and Forbes (2014*) , also analyzing the 2002-2011 SABER data, arrive at a variation in the interannual amplitude with minima in 2008 and 2009, similar to that by *Gu et al.* (*2013*). *Tunbridge et al. (2011)*, from MLS temperature data between 2004 and 2009 also obtain similar results, with W3 amplitudes reaching 12 K, and with the weakest amplitudes in 2008 and 2009. These interannual behaviours are more or less consistent with the present results between 2008 and 2012 (Fig. 9). Amplitudes that exceeded 17 K (Fig. 12) – somewhat higher than those shown by *Gu et al.* (2013) – were obtained for some dates in January 2012 in the present study.

Here it was found that there is no increase in the amplitude of temperatures with altitude but rather, a slight decrease: the mean growth factor between the OH layer and the O_2 layer is 0.95 (±0.04). This differs greatly from the growth factor for the semidiurnal tide which is 1.42 (±0.04) (see *Reisin and Scheer, 2019*).

There are few precedents in the literature regarding QTDWs in airglow intensities. With data from Cachoeira Paulista (22.7º S, 45.0º W) between March and November 1999 (summer months not included), *Takahashi et al. (2005),* observe a clear maximum amplitude of OH intensity during July (see their Fig. 4c). Although based on a few cases, the present OH intensities do not appear to support this July peak because the amplitude level is similar to that of August and October (Fig. 6).

Hecht et al. (2010) analyzed the QTDWs with OH and O_2 data from January 25 to February 5, 2003, measured at two sites in Australia in latitudes similar to El Leoncito. Using pairs of consecutive nights, they obtain the relative variation of intensities and temperatures ($\Delta I / I$ and $\Delta T / T$) and the corresponding $|\eta|$ value for each date (see their Tables 2 - 5). These values are strongly variable from day to day. Excluding the

outliers, $\Delta I / I$ values are typically in the range between 25% and 55% for both emissions, similar to the January averages shown here (Fig. 11). *Hecht et al. (2010)* argue that the response to QTDW in airglow intensity is much greater than the response in temperature or, in other words, $|\eta| >> 1$. As in the case of $\Delta I / I$, the values of $|\eta|$ also have a strong day-to-day variability. From the Alice Springs data (see their Tables 4 and 5), $|\eta|$ medians are close to 11 for both emissions. That is, the values of $|\eta|$ tend to be even higher than those shown here (Fig. 7). On the other hand, *Hecht et al. (2010)* also mention that "airglow intensity and temperature are generally in phase, with an uncertainty of a few hours", which is consistent with the present results.

Another study of planetary waves based on the same OH and O_2 emission bands was done by *López-González et al. (2009)*, using data acquired between 1998 and 2007 with the Spectral Airglow Temperature Imager (SATI) installed at Sierra Nevada Observatory (37.06º N, 3.38º W). They divide their results into four different period ranges (around 2-days, 5-days, 10-days, and 16-days). The probability of the presence of 2-day waves with respect to the month is very different from that observed in this paper: for O_2 temperatures almost all the cases detected correspond to the northern winter months (January to March) while for the OH temperatures, the detected waves extend between both solstices (January to August). This different seasonal behaviour is not unexpected considering that these are measurements in the opposite hemispheres.

The QTDWs found here often have a long vertical wavelength, especially in the O_2 layer. However, waves with vertical wavelengths from 20 km have also been detected. Upward waves with long vertical wavelengths ($|\lambda_z| > 100$ km) were already found in wind measurements at Kyoto (35ºN) and Adelaide (35ºS) by *Tsuda et al. (1988)*. In the recent paper based on wind measurements with a network of eight radars between 23ºS and 76ºS in January 2015, *Fritts et al.* (2019) determine QTDWs with $|\lambda_z|$ between 75 and 100 km at mid-latitude sites and with even longer $|\lambda_z|$ (> 150 km) at high-latitude sites. *Guharay et al. (2012)*, using wind measurements with the meteor radar in Santa María (29.7° S, 53.7° W) in the summers of 2005-2007, obtain mean vertical wavelengths with values of ~ 62 km for zonal wind and ~74 km for meridional wind. Using wind data measured in Cachoeira Paulista, *Lima et al. (2004)* found vertical wavelengths varying in the range of 40-140 km during the months of January and February from 2000 to 2002. Vertical wavelengths shorter than those observed here, between 40 and 80 km, have been shown by *Huang et al. (2013*, see their Fig. 4) from the SABER temperatures at 32ºS during January-February 2003. Similar results ($|\lambda_z| <$ 60 km) from SABER temperatures of 2003-2005 is shown for 30ºS by *Ern et al.* (2013, see their Fig. 6a).

5. Summary

From the large database of OH and O_2 intensities and temperatures acquired from El Leoncito and using strict selection criteria, it was possible to obtain several characteristics of the quasi-two-day waves in this location, between 2006 and 2020 (and two isolated cases in December 2002). The method is only applied to the cases in which the QTDW is the strongest planetary wave. These are the main results:

- In January, the QTDW is the strongest planetary wave, and it is strong in the other summer months. For the rest of the months, the occurrence of strong QTDWs is much less frequent.

- The waves detected are mainly included in the period range of 45-52 hours. For January only, the distribution of periods is limited to a narrower range, with most of the cases between 45 and 48 hours and medians somewhat less than 2 days (~ 46 hours).
- On average, the amplitude of the January temperature oscillations are greater than 10 K in both emission layers, exceeding, by at least 3 K, the corresponding values of the neighbouring months.
- For the January cases in which QTDW is detected in both emissions, the temperature amplitude is slightly greater in the OH layer ($A_{TO2}/A_{TOH} = 0.95 \pm 0.04$, on average).
- QTDW affects intensities much more strongly than temperatures. The monthly averages of the relative intensity amplitudes vary between 15% and 43%, reaching the peak in January.
- From year to year, there is a great variability of the January amplitude averages. Among the nine documented years (2008-2012, 2014-2015 and 2019-2020), the first three were of lower temperature amplitudes (with the minimum in 2009 having an OH amplitude of ~5 K) and the maximum in 2012 (~14 K for O_2 and ~12.5 K for OH). For the relative intensity amplitudes, 2009 and 2012 were also the years with extreme values of ~18% and ~47%, respectively.
- The day-to-day evolution of QTDW is different in each of the four observed parameters.
- In both emissions, the Krassovsky's η ratios are completely distributed in the first and fourth quadrant of the complex plane, with an accumulation of cases close to the real axis. The mean vector of η has a modulus of 6.14 (±0.15) and phase of 0.02º (±1.44º) for OH, and 8.08 (±0.11) and -3.80º (±0.79º) for O_2.
- The detected QTDWs tend to have a long vertical wavelength (greater than 100 km), especially in the O_2 layer. However, also cases of shorter vertical wavelength (from $|\lambda_z| > 20$ km) and with both directions of vertical propagation have also been observed.

Many of the results obtained here are consistent with those discussed in the literature for similar latitudes to El Leoncito. With a method similar to that used in the past to study the semidiurnal tide, it has been shown how, from airglow data, it is possible to extract valuable information about the QTDW.

Acknowledgments:

Based on data obtained at Complejo Astronómico El Leoncito, operated under agreement between the Consejo Nacional de Investigaciones Científicas y Técnicas de la República Argentina and the National Universities of La Plata, Córdoba and San Juan. The permanent technical support of CASLEO staff is appreciated. Funding by the Argentine CONICET PUE-IAFE and PIP 11220130100439CO, and the Argentine ANPCyT PICT-2016-0221 is acknowledged.

References.

Baker, D.J., Stair Jr., A.T., 1988. Rocket measurements of the altitude distributions of the hydroxyl airglow. Phys. Scripta, 37(4), 611-622.

Chang, L.C., Yue, J., Wang, W., Wu, Q., Meier, R.R., 2014. Quasi-two day wave related variability in the background dynamics and composition of the mesosphere / thermosphere, and the ionosphere. J. Geophys. Res., 119, 4786-4804, doi:10.1002/2014JA019936.

Chshyolkova, T., Manson, A.H., Meek, C.E., 2005. Climatology of the quasi two-day wave over Saskatoon (52°N, 107°W): 14 Years of MF radar observations. Adv. Space Res., 35(11), 2011-2016.

Clark, R.R., 1975. Meteor wind measurements at Durham, New Hampshire (43ºN, 71ºW). J. Atmos. Terr. Phys., 32, 1689-1693.

Efron, B., Gong, G., 1983. A leisurely look at the bootstrap, the jackknife, and cross-validation. The American Statistician, 37(1), 36-48.

Ern, M., Lehmann, C., Kaufmann, M., Riese, M., 2009. Spectral wave analysis at the mesopause from SCIAMACHY airglow data compared to SABER temperature spectra. Ann. Geophys., 27, 407-416.

Ern, M., Preusse, P., Kalisch, S., Kaufmann, M., Riese, M., 2013. Role of gravity waves in the forcing of quasi two-day waves in the mesosphere: An observational study. J. Geophys. Res., 118, 3467-3485, doi:10.1029/2012JD018208.

Forbes, J.M., Moudden, Y., 2012. Quasi-two-day wave-tide interactions as revealed in satellite observations. J. Geophys. Res., 117(D12), D12110, doi:10.1029/2011JD017114.

Fritts, D.C., Iimura, H., Janches, D., Lieberman, R.S., Riggin, D.M., Mitchell, N.J., Vincent, R.A., Reid, I.M., Murphy, D.J., Tsutsumi, M., Kavanagh, A.J., Batista, P., Hocking, W.K., 2019. Structure, variability, and mean-flow interactions of the January 2015 quasi-2-day wave at middle and high Southern latitudes. J. Geophys. Res., 124, 5981-6008, doi:10.1029/2018JD029728.

Gaikwad, H.P., Sharma, A.K., Gurav, O.B., Chavan, G.A., Nade, D.P., Patil, P.T., Nikte, S.S., Naniwadekar, G.P., 2019. Seasonal, annual and inter-annual variability in MLT Quasi Two Day Waves over low latitude region Kolhapur (16.8°N; 74.2°E). Adv. Space Res., 63, 2100-2117, doi:10.1016/j.asr.2018.12.029.

Glass, M., Fellous, J.L , Massebeuf, M , Spizzichino, A., Lysenko, I.A., Portnyagin, Yu.I., 1975. Comparison and interpretation of the results of simultaneous wind measurements in the lower thermosphere at Garchy (France) and Obninsk (U.S.S.R.) by meteor radar technique. J. Atmos. Terr. Phys., 37, 1077-1087.

Gu, S.-Y., Li, T., Dou, X., Wu, Q., Mlynczak, M.G., Russell III, J.M., 2013. Observations of quasi-two-day wave by TIMED/SABER and TIMED/TIDI. J. Geophys. Res., 118, 1624-1639, doi:10.1002/jgrd.50191.

Gu, S.-Y., Dou, X.-K., Yang, C.-Y., Jia, M., Huang, K.-M., Huang, C.-M., Zhang, S.-D., 2019. Climatology and anomaly of the quasi-two-day wave behaviors during 2003-2018 austral summer periods. J. Geophys. Res., 124, 544-556, doi:10.1029/2018JA026047.

Guharay, A., Batista, P.P., Clemesha, B.R., Schuch, N.J., 2012. Study of the quasi-two-day wave during summer over Santa Maria, Brazil using meteor radar observations. J. Atmos. Solar-Terr. Phys., 92, 83-93, doi:10.1016/j.jastp.2012.10.005.

Guharay, A., Batista, P.P., Clemesha, B.R., 2015. Variability of the quasi-2-day wave and interaction with longer period planetary waves in the MLT at Cachoeira Paulista (22.7°S, 45°W). J. Atmos. Solar-Terr. Phys., 130-131, 57-67, doi:10.1016/j.jastp.2015.05.010.

Gurubaran, S., Sridharan, S., Ramkumar, T.K., Rajaram, R., 2001. The mesospheric quasi-2-day wave over Tirunelveli (8.7°N). J. Atmos. Solar-Terr. Phys., 63, 975-985.

Hecht, J.H., Walterscheid, R.L., Gelinas, L.J., Vincent, R.A., Reid, I.M., Woithe, J.M., 2010. Observations of the phase-locked 2 day wave over the Australian sector using medium-frequency radar and airglow data. J. Geophys. Res., 115(D16), D16115, doi:10.1029/2009JD013772.

Hines, C.O., Tarasick, D.W., 1987. On the detection and utilization of gravity waves in airglow studies. Planet. Space Sci., 35(7), 851-866.

Huang, Y.Y., Zhang, S.D., Yi, F., Huang, M., Gan, Q, Gong, Y., 2013. Global climatological variability of quasi-two-day waves revealed by TIMED/SABER observations. Ann. Geophys., 31, 1061-1075.

Jacobi, Ch., Portnyagin, Yu.I., Merzlyakov, E.G., Kashcheyev, B.L., Oleynikov, A.N., Kürschner, D., Mitchell, N.J., Middleton, H.R., Muller, H.G., Comley, V.E., 2001. Mesosphere/lower thermosphere wind measurements over Europe in summer 1998. J. Atmos. Solar-Terr. Phys., 63, 1017-1031.

Lilienthal, F., Jacobi, Ch., 2015. Meteor radar quasi 2-day wave observations over 10 years at Collm (51.3ºN, 13.0ºE). Atmos.Chem.Phys., 15, 9917-9927, doi:10.5194/acp-15-9917-2015.

Lima, L.M., Batista, P.P., Takahashi, H., Clemesha, B.R., 2004. Quasi-two-day wave observed by meteor radar at 22.7°S. J. Atmos. Solar-Terr. Phys., 66(6-9), 529-537.

Liu, G., England, S.L., Janches, D., 2019. Quasi two-, three-, and six-day planetary-scale wave oscillations in the upper atmosphere observed by TIMED/SABER over ~17 years during 2002-2018. J. Geophys. Res., 124, 9462-9474, doi:10.1029/2019JA026918.

López-González, M.J., Rodríguez, E., García-Comas, M., Costa, V., Shepherd, M.G., Shepherd, G.G., Aushev, V.M., Sargoytchev, S., 2009. Climatology of planetary wave type oscillations with periods of 2-20 days derived from O_2 atmospheric and OH(6-2) airglow observations at mid-latitude with SATI. Ann. Geophys., 27, 3645-3662.

Ma, Z., Gong, Y., Zhang, S., Zhou, Q., Huang, C., Huang, K., Yu, Y., Li, G., Ning, B., Li, C., 2017. Responses of quasi 2 day waves in the MLT region to the 2013 SSW revealed by a meteor radar chain. Geophys. Res. Lett., 44, 9142-9150, doi:10.1002/2017GL074597.

Malinga, S.B., Ruohoniemi, J.M., 2007. The quasi-two-day wave studied using the Northern Hemisphere SuperDARN HF radars. Ann. Geophys., 25, 1767-1778.

McCormack, J.P., Coy, L., Hoppel, K.W., 2009. Evolution of the quasi 2-day wave during January 2006. J. Geophys. Res., 114(D20), D20115, doi:10.1029/2009JD012239.

Meek, C.E., Manson, A.H., Franke, S.J., Singer, W., Hoffmann, P., Clark, R.R., Tsuda, T., Nakamura, T., Tsutsumi, M., Hagan, M., Fritts, D.C., Isler, G., Portnyagin, Yu.I., 1996. Global study of northern hemisphere quasi-2-day wave events in recent summers near 90 km altitude. J. Atmos. Terr. Phys., 58, 1401-1411.

Moudden, Y., Forbes, J.M., 2014. Quasi-two-day wave structure, interannual variability and tidal interactions during the 2002-2011 decade. J. Geophys. Res., 119, 2241-2260, doi:10.1002/2013JD020563.

Muller, H.G., Nelson, L., 1978. A travelling quasi 2-day wave in the meteor region. J. Atmos. Terr. Phys., 40, 761-766.

Namboothiri, S.P., Kishore, P., Igarashi, K., 2002. Observations of the quasi-2-day wave in the mesosphere and lower thermosphere over Yamagawa and Wakkanai. J. Geophys. Res., 107, 4320, doi:10.1029/2001JD000539.

Nguyen, V.A., Palo, S.E., Lieberman, R.S., Forbes, J.M., Ortland, D.A., Siskind, D.E., 2016. Generation of secondary waves arising from nonlinear interaction between the quasi 2 day wave and the migrating diurnal tide. J. Geophys. Res., 121, 7762-7780, doi:10.1002/2016JD024794.

Nozawa, S., Brekke, A., Maeda, S., Aso, T., Hall, C.M., Ogawa, Y., Buchert, S.C., Röttger, J., Richmond, A.D., Roble, R., Fujii, R., 2005. Mean winds, tides, and quasi-2 day wave in the polar lower thermosphere observed in European Incoherent Scatter (EISCAT) 8 day run data in November 2003. J. Geophys. Res., 110(A12), A12309, doi:10.1029/2005JA011128.

Palo, S.E., Avery, S.K., 1996. Observations of the quasi-two-day wave in the middle and lower atmosphere over Christmas Island. J. Geophys. Res., 101, 12833-12846.

Palo, S.E., Forbes, J.M., Zhang, X., Russell III, J.M., Mlynczak, M.G., 2007. An eastward propagating two-day wave: Evidence for nonlinear planetary wave and tidal coupling in the mesosphere and lower thermosphere. Geophys. Res. Lett., 34, L07807, doi:10.1029/2006GL027728.

Pancheva, D.V., 2006. Quasi-2-day wave and tidal variability observed over Ascension Island during January/February 2003. J. Atmos. Solar-Terr. Phys., 68(3-5), 390-407.

Pancheva, D., Mukhtarov, P., Siskind, D.E., 2018. Climatology of the quasi-2-day waves observed in the MLS/Aura measurements (2005-2014). J. Atmos. Solar-Terr. Phys., 171, 210-224.

Pedatella, N.M., Forbes, J.M., 2012. The quasi 2 day wave and spatial-temporal variability of the OH emission and ionosphere. J. Geophys. Res., 117(A1), A01320, doi:10.1029/2011JA017186.

Pendlebury, D., 2012. A simulation of the quasi two-day wave and its effect on variability of summertime mesopause temperatures. J. Atmos. Solar-Terr. Phys., 80, 138-151.

Plumb, R.A., Vincent, R.A., Craig, R.L., 1987. The quasi-two-day wave event of January 1984 and its impact on the mean mesospheric circulation. J. Atmos. Sci., 44, 3030-3036.

Reisin, E.R., Scheer, J., 1996. Characteristics of atmospheric waves in the tidal period range derived from zenith observations of O_2*b*(0-1) Atmospheric and OH(6-2) airglow at lower midlatitudes. J. Geophys. Res., 101, 21223-21232.

Reisin, E.R., Scheer, J., 2019. The semidiurnal tide for individual nights derived consistently from O_2 and OH intensities and temperatures. J. Atmos. Solar-Terr. Phys., 186, 20-27.

Salby, M.L., 1981. The 2-day wave in the middle atmosphere: Observations and theory. J. Geophys. Res., 86, 9654-9660.

Scheer, J., 1987. Programmable tilting filter spectrometer for studying gravity waves in the upper atmosphere. Appl. Opt., 26, 3077-3082.

Scheer, J., Reisin, E.R., 2001. Refinements of a classical technique of airglow spectroscopy. Adv. Space Res., 27(6-7), 1153-1158.

Suresh Babu, V., Kishore Kumar, K., John, S.R., Subrahmanyam, K.V., Ramkumar, G., 2011. Meteor radar observations of short-term variability of quasi 2 day waves and their interaction with tides and planetary waves in the mesosphere-lower thermosphere region over Thumba (8.5°N, 77°E). J. Geophys. Res., 116(D16), D16121, doi:10.1029/2010JD015390.

Takahashi, H., Lima, L.M., Wrasse, C.M., Abdu, M.A., Batista, I.S., Gobbi, D., Buriti, R.A., Batista, P.P., 2005. Evidence on 2-4 day oscillations of the equatorial ionosphere h'F and mesospheric airglow emissions. Geophys. Res. Lett., 32(12), L12102, doi:10.1029/2004GL022318.

Tsuda, T., Kato, S., Vincent, R.A., 1988. Long period wind oscillations observed by the Kyoto meteor radar and comparison of the quasi-2-day wave with Adelaide HF radar observations. J. Atmos. Terr. Phys., 50, 225-230, doi:10.1016/0021-9169(88)90071-2.

Tunbridge, V.M., Mitchell, N.J., 2009. The two-day wave in the Antarctic and Arctic mesosphere and lower thermosphere. Atmos.Chem.Phys., 9, 6377-6388, doi:10.5194/acp-9-6377-2009.

Tunbridge, V.M., Sandford, D.J., Mitchell, N.J., 2011. Zonal wave numbers of the summertime 2 day planetary wave observed in the mesosphere by EOS Aura Microwave Limb Sounder. J. Geophys. Res., 116(D11), D11103, doi:10.1029/2010JD014567.

Venkateswara Rao, N., Venkat Ratnam, M., Vedavathi, C., Tsuda, T., Krishna Murty, B.V., Satishkumar, S., Gurubaran, S., Kishore Kumar, K., Subrahmanyam, K.V., Vijaya Bhaskara Rao, S., 2017. Seasonal, inter-annual and solar cycle variability of the quasi two day wave in the low-latitude mesosphere and lower thermosphere. J. Atmos. Solar-Terr. Phys., 152, 20-29, doi:10.1016/j.jastp.2016.11.005.

Walterscheid, R.L., Vincent, R.A., 1996. Tidal generation of the phase-locked 2-day wave in the southern hemisphere summer by wave-wave interactions. J. Geophys. Res., 101, 26557-26576, doi:10.1029/96JD02248.

Wang, J.C., Chang, L.C., Yue, J., Wang, W., Siskind, D.E., 2017. The quasi 2 day wave response in TIME-GCM nudged with NOGAPS-ALPHA. J. Geophys. Res., 122, 5709-5732, doi:10.1002/2016JA023745.

Witt, G., Stegman, J., Solheim, B.H., Llewellyn, E.J., 1979. A measurement of the $O_2(b^1\Sigma_g^+ - X^3\Sigma_g^-)$ atmospheric band and the OI (^1S) green line in the nightglow. Planet. Space Sci., 27, 341-350.

Xiong, J., Wan, W., Ding, F., Liu, L., Hu, L., Yan, C., 2018. Two-day wave travelling westward with wavenumber one during the sudden stratospheric warming in January 2017. J. Geophys. Res., 123, 3005-3013, doi:10.1002/2017JA025171.

Yue, J., Liu, H.-L., Chang, L.C., 2012. Numerical investigation of the quasi 2 day wave in the mesosphere and lower thermosphere. J. Geophys. Res., 117(D5), D05111, doi:10.1029/2011JD016574.